DEUTSCHES ELEKTRONEN-SYNCHROTRON
INSTITUT FÜR HOCHENERGIEPHYSIK

DESY 93-159
INFN/AE-93/21
November 1993

Test Beam Results from the Prototype L3 Silicon Microvertex Detector

A. Adam et al.

ISSN 0418-9833

PLATANENALLEE 6 - 15738 ZEUTHEN

To be sure that your preprints are promptly included in the HIGH ENERGY PHYSICS INDEX, send them to (if possible by air mail):

DESY **Bibliothek** **Notkestraße 85** **22603 Hamburg** **Germany**	**DESY-IfH** **Bibliothek** **Platanenallee 6** **15738 Zeuthen** **Germany**

DESY 93-159
INFN/AE-93/21
November 1993

ISSN 0418-9833

Test Beam Results from the Prototype L3 Silicon Microvertex Detector

A.Adam[5] O.Adriani[6] S.Ahlen[1] G.Ambrosi[13] E.Babucci[13] L.Baksay[16] A.Baschirotto[12] R.Battiston[13,8] A.Bay[9] Gy.L.Bencze[5] B.Bertucci[13] M.Biasini[13] G.M.Bilei[13] G.J.Bobbink[2] M.Bosetti[12] M.L.Brooks[11] W.J.Burger[9] J.Busenitz[16] C.Camps[1] M.Caria[13] G.Castellini[7] R.Castello[12] B.Checcucci[13] A.Chen[14] T.E.Coan[11] V.Commichau[1] D.DiBitonto[16] P.Duinker[2] S.Easo[13] P.Extermann[9] E.Fiandrini[13] A.Gabbanini[7] A.Gougas[3] K.Hangarter[1] C.Hauviller[8] A.Herve[8] G.Hu[20] M.I.Josa[8] J.S.Kapustinsky[11] D.Kim[3] W.W.Kinnison[11] J.Kornis[5] V.R.Krastev[13] G.Landi[6] M.Lebeau[8] D.M.Lee[11] R.Leiste[1,18] W.Lin[14] W.Lohmann[17] A.Marin[4] R.Massetti[13] G.Matay[5] G.B.Mills[11] H.Nowak[17] G.Passaleva[5,13] T.Paul[3] M.Pauluzzi[13] S.Pensotti[12] E.Perrin[9] P.G.Rancoita[12] M.Rattaggi[12] A.Rosch[1] A.Santocchia[13] R.Siedling[1] M.Sachwitz[17] P.Schmitz[9] B.Schöneich[17] L.Servoli[13] G.F.Susinno[9] G.Terzi[12] M.Tesi[7] F.Tonisch[17] J.Toth[5] G.Trowitzsch[17] G.Viertel[18] H.Vogt[17] S.Waldmeier[18] J.Wegmann[17] R.Weill[10] J.Xu[4] S.C.Yeh[15] B.Zhou[4]

1 I. Physikalisches Institut, RWTH, D-52056 Aachen, FRG
III. Physikalisches Institut, RWTH, D-52056 Aachen, FRG
2 National Institute for High Energy Physics, NIKHEF, NL-1009 DB Amsterdam, The Netherlands CEDEX , France
3 Johns Hopkins University, Baltimore, MD 21218, USA
4 Boston University, Boston, MA 02215, USA
5 Central Research Institute for Physics of the Hungarian Academy of Sciences, H-1525 Budapest 114, Hungary
6 INFN Sezione di Firenze and University of Florence, I-50125 Florence, Italy
7 INFN Sezione di Firenze and Instituto Ricerca Onde Elettromagnetiche, I-50125 Florence, Italy
8 European Laboratory for Particle Physics, CERN, CH-1211 Geneva 23, Switzerland
9 University of Geneva, CH-1211 Geneva 4, Switzerland
10 University of Lausanne, CH-1015 Lausanne, Switzerland
11 Los Alamos National Laboratory, Los Alamos, NM 87544, USA
12 INFN-Sezione di Milano, I-20133 Milan, Italy
13 INFN-Sezione di Perugia and Universitá Degli Studi di Perugia, I-06100 Perugia, Italy
14 National Central University, Chung-li, Taiwan
15 National Tsing Hua University, Hsinchu, Taiwan
16 University of Alabama, Tuscaloosa, AL 35486, USA
17 DESY-Institut für Hochenergiephysik, D-15738 Zeuthen, FRG
18 Eidgenössische Technische Hochschule, ETH Zürich, CH-8093 Zürich, Switzerland
19 Permanent address : Laboratoire d'Annecy-le-Vieux de Physique des Particules, LAPP, IN2P3-CNRS, BP 110, F-74941 Annecy-le-Vieux
20 Present address : World Laboratory, FBLJA Project, CH-1211 Geneva 23 Switzerland

Abstract

We report test beam results on the overall system performance of two modules of the L3 Silicon Microvertex Detector exposed to a 50 GeV pion beam. Each module consists of two AC coupled double-sided silicon strip detectors equipped with VLSI readout electronics. The associated data acquisition system comprises an 8 bit FADC, an optical data transmission circuit, a specialized data reduction processor and a synchronization module. A spatial resolution of 7.5 μm and 14 μm for the two coordinates and a detection efficiency in excess of 99% are measured.

1 Introduction

A Silicon Microvertex Detector (SMD) has been recently installed as the inner most position of the central tracker of the L3 experiment at the CERN LEP storage ring.

Sectional views of L3's tracking system are shown in the upper part of Fig. 1. A high resolution drift chamber working in the time expansion mode [1] (TEC) provides multiple coordinate measurement in the Φ plane. Two multiwire proportional chambers with cathode strip readout [2] are placed at the outer radius of the TEC and deliver two Z-coordinate measurements. As can be seen from the lower part of Fig. 1 the SMD consists of two cylindrical shells of double-sided silicon microstrip sensors surrounding the beam pipe at radii of about 6 cm and 8 cm. The sensors measure the spatial coordinates of charged particles over the polar angle range $22° \leq \Theta \leq 158°$ and over the full azimuth. A detailed description of the SMD design can be found in reference [3].

Precision measurements on charged tracks close to the interaction point will improve L3's current momentum, impact parameter and polar angle resolutions, essential for b-quark tagging and W-boson studies at LEP200.

Our test beam experiment was performed to gain experience operating the complete system of sensors, front-end electronics, cooling system, position monitoring systems and data acquisition chain. We measured the spatial resolution, detection efficiency, cluster size distribution and signal to noise ratio of the silicon sensors.

2 The Prototype Detector

Two modules of the SMD were installed during summer 1992 in a test beam of 50 GeV pions. For the first time, prototypes of all components of the system, corresponding to 1/24 of the actual SMD, were set up. We now describe the main components.

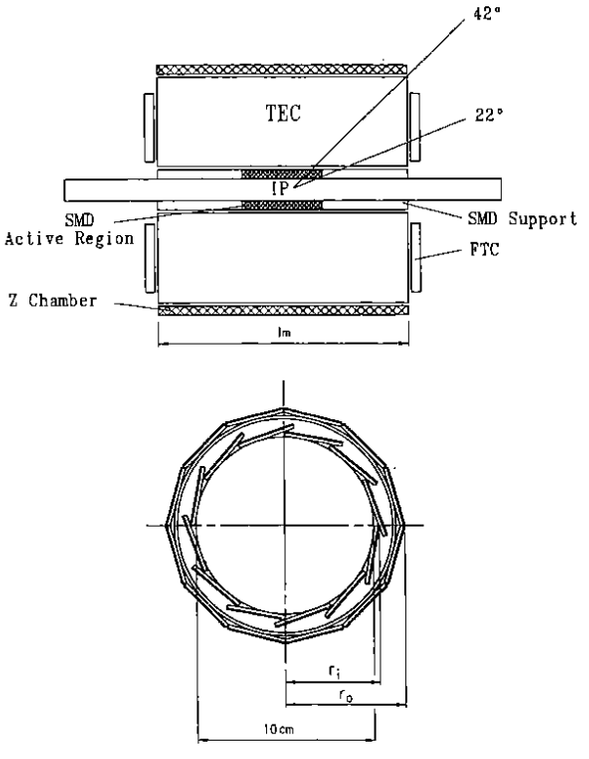

Figure 1: *Sectional views of the tracking system of the L3 detector*

2.1 The Detector Modules

Figure 2 shows a detector module. A module consists of 2 consecutive silicon sensors of planar size $\sim 7 \times 4\,\mathrm{cm}^2$ and 300 μm thickness. The Φ-measuring strips run the full length on one side of the module while on the other side are orthogonal z-measuring strips.

The sensors are fabricated [4] on a design by INFN Pisa [5] from n-doped silicon wafers of resistivity $\geq 6\,\mathrm{k}\Omega$- cm and fully depleted between 30 and 50 V. The implantation strip pitch is 25 μm on the diode (Φ-measuring) side and 50 μm on the ohmic (Z-measuring) side. The

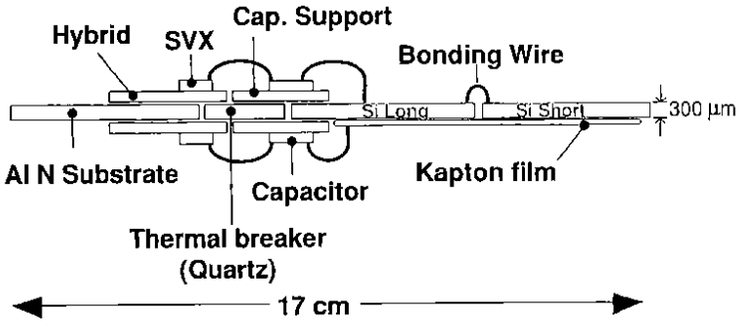

Figure 2: *Schematical view of the SMD module as used in the testbeam.*

readout pitch is 50 μm on the Φ-measuring side and, depending on the polar angle, 150 or 200 μm on the Z-measuring side. A detailed description can be found in [6].

The readout electronics for both sensor sides are placed at the same end of the module. The Φ-side readout strips are AC-coupled to the preamplifiers by a special integrated 150 pF capacitor built on a quartz substrate.

The signals from the Z-side strips are transmitted to the AC coupling capacitors of the readout electronics by a special flex cable made from 2.5μm thick, L-shaped copper strips plated onto a 50μm thick kapton foil. [7]

2.2 The Readout Electronics

The strips on both sides of the sensors are read out by an electronics chain consisting of charge sensitive preamplifiers, an auxiliary electronics board, an analog to digital converter and an optical transmission line to the data acquisition system. A special synchronization module receives external triggers and synchronizes the components of the electronics chain (Fig.3).

At the end of each module farthest from the interaction point, a hybrid carrying six SVX-H chips is glued to each side of the module (Fig.2). The SVX-H is a specially developed VLSI radiation hard chip [8] fabricated using a 1.2 μm CMOS technology [9]. The chip comprises an analog and a digital section. The analog section contains 128 channels of low-noise charge sensitive amplifiers with a gain of $\sim$ 25 mV/fC. The digital section part controls the multiplexed readout and loads channel and chip identification onto a digital bus. A detailed testing procedure for the choice of the SVX-H chips can be found in [10].

The six SVX chips on each hybrid are daisy-chained and read out by an intermediate electronics board, the 'Converter', placed near the detector. The Converter contains an amplifier to drive the analog data, low drop voltage regulators for the SVX analog and digital power and bidirectional line drivers for the SVX control and digital bus.

Analog and digital data are received from and sent to a special optical transceiver board (Optoboard) [11] placed at a 10 m distance from the detector. On the Optoboard the analog signals are digitized by an 8 bit 40 MHz flash ADC. All output data are sent by a 120 m optical fiber to an optical receiver at the front-end of the data acquisition system. The optical transmission decouples the detector and readout electronics from the data acquisition. This is done because the detector's Φ and Z sides are at different potentials and to reduce ground loop problems.

2.3 The Data Acquisition System

The Data Acquisition System (DAQ) of the SMD (Fig. 3) is a branch of VME crates. Each crate is controlled by a Crate Master [12] which communicates with special Data Reduction Processors (DRPs) [13] in its crate and transfers their data to the data acquisition (DAQ) stream. The DRPs contain a processor chip and random access memory for programming, data and event buffering. Each DRP receives data from one daisy chain of up to 12 SVX chips and writes it to a fast memory.

The programs [14] running on the DRP handle different output modes. We used the raw

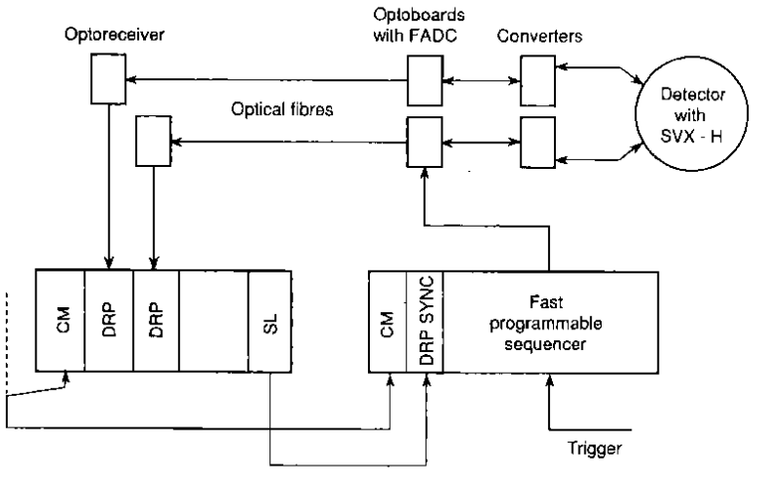

Figure 3: *Read out and data acquisition scheme*

mode in which the ADC contents of all channels of a SVX chain are transferred to the DAQ stream.

The synchronization of the readout to the external trigger is achieved by the Sequencer [15] which generates bit patterns necessary to start and synchronize the multiplexed readout of the SVX to the DRPs. Its central part is a micro-processor and a fast RAM. The memory contains the instructions and the output patterns which are sent to both the optoboard and the VME bus. The Sequencer generates patterns for pedestal taking, calibration and data taking.

A VAX cluster was used to assemble and download programs to the different levels of the DAQ system. It received and wrote data to a tape unit and served as the user front end.

3 Displacement Monitoring Systems

The real SMD has two independent systems to measure the relative angular and translational displacements of the SMD with respect to the rest of the L3 central tracker. One system is a laser displacement monitoring system (LDMS) and the other is a capacitive displacement monitoring system (CDMS). To test the operation of these systems during data taking we installed prototypes of the LDMS and CDMS along with our prototype detector modules.

The LDMS consists of a laser diode, optical fibers and lenses. The laser diode produces short pulses of infrared (905 nm) light transmitted by an optical fiber to a lens-prism assembly which finally directs the light onto the silicon sensors, illuminating several adjacent strips. The strips are then read out by the standard DAQ system. A change in the centroid of the light spot indicates a relative motion of a sensor with respect to the external mechanical frame holding the lens-prism assembly.

The CDMS monitors long term radial and transverse displacements. A single channel utilizes a sensor [16], mounted on the detector mechanical frame, facing a grounded electrode placed on the external support. The sensor is instrumented by electronics which (a) excites the sensor with an AC current of fixed frequency and constant magnitude and (b) measures and processes the potential difference between the sensor and ground target to produce an essentially DC output voltage which varies inversely with the capacitance between sensor and ground electrode. This voltage is digitized by a CAMAC ADC/MUX system [17] and read out once per minute.

4 Cooling

The 10 μm design tolerance on positional errors for the actual SMD requires a very stable temperature. Consequently, we have cooled the prototype detectors in the same manner as foreseen in L3 and monitored their temperature stability. The total power dissipated by both the Converters and the SVX-H chips is about 0.5 W/cm^2, approximately 15 W for both test

modules.

The Converters were cooled by placing thin water cooled plates 1 mm above them and flowing 10 liters/hr of water through narrow aluminum pipes attached to the plates. The hybrids holding the SVX chips were cooled by flowing 10 liters/hr of water through a channel machined into the aluminum mechanical flange supporting the hybrids. All cooling circuits were under partial vacuum to prevent fluid loss if a leak developed.

The temperature of the front end electronics and the sensors was monitored through platinum wire resistance thermometers glued to the mechanical support structure of the modules.

5 Test Beam Set Up

Two modules, fully equipped with readout electronics, were installed in the X-3 test beam line at CERN. The modules were irradiated with 50 GeV pions during spills of 2.5 second duration, producing about 5 triggers per spill, roughly uniform in time. More than 10^5 triggers were written to tape at incident polar angles of 0°, 10°, 20° and 30°.

The overall scheme of the test setup is shown in Fig. 4. Two modules were placed on a replica of the real SMD mechanical structure. The modules had a relative position corresponding to an azimuthal wedge of the actual SMD. The replica is positioned inside a mock-up of the TEC. The mock-up could be rotated with respect to the beamline to measure detector performance as a function of the polar angle Θ. It also held portions of the two displacement monitor systems. Upstream and downstream of the modules were trajectory defining reference silicon strip detectors. These single-sided detectors had an active area between $13 \times 13\,\mathrm{mm}^2$ and $16 \times 60\,\mathrm{mm}^2$, a readout pitch of either 50 μm or 60 μm and measured positions along 2 axes perpendicular to the beam axis. They were read out by SVX-D chips and had their analog signals digitized by a 6 bit FADC and then transferred to a DRP.

A beam particle trigger was formed by 2 pairs of scintillator paddles, one pair upstream and one pair downstream of the modules under study. The DAQ trigger was the logical AND of

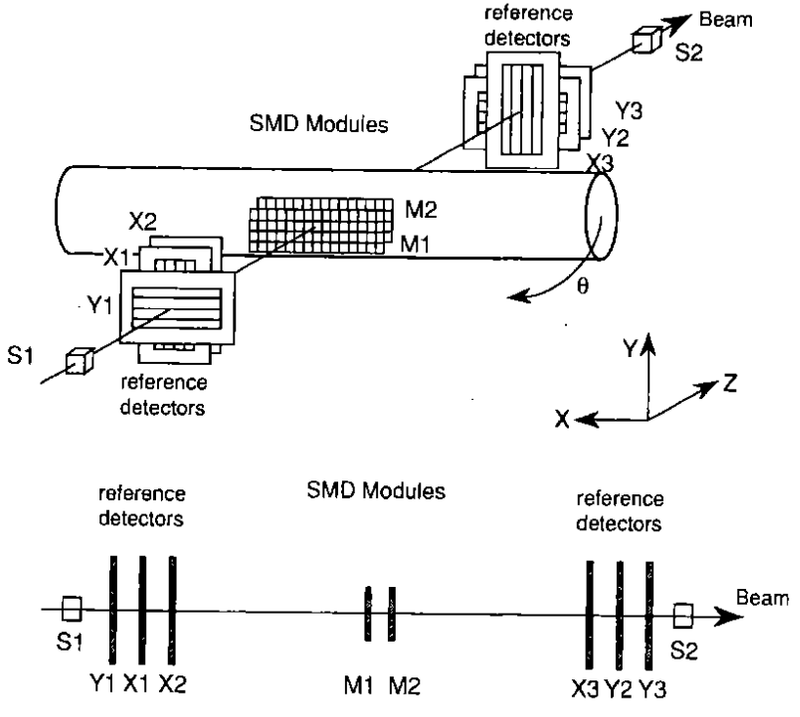

Figure 4: *The test beam set-up*

all four scintillators.

6 Offline Analysis and Results

All components of the Data Acquisition System were running in raw data mode. Hence, the calculation of pedestals and their rms values, the selection of valid clusters, the calculation of hit coordinates and the determination of efficiency and spatial resolution were all done offline [18]. Data from the LDMS, the CDMS and the cooling system were also recorded.

We start the analysis by first determining, on an event by event basis, the significant common mode noise observed on all channels of a given SVX. Here, the common mode noise is defined to be the average pulse height per event per SVX, care being taken to exclude non-working channels and possible signals from the average. Next, this common mode noise is subtracted from the pulse height of each channel and the residual is then averaged over 100 triggers to obtain the pedestal and its root mean square for each channel.

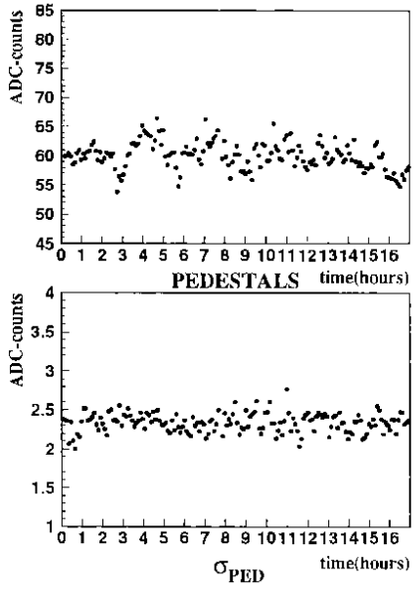

Figure 5: *Pedestal and σ_{ped} behavior over 16 hours*

As can be seen from Fig.5 we observed over periods of 16 hours a pedestal variation greater than its rms. We therefore applied an event by event adjustment [19] of the pedestals to account for slow coherent pedestal drifts.

6.1 Charge Cluster and Signal to Noise Ratio

Various selection criteria were applied in order to separate signals from noise. The following procedure gave the best results. For every trigger, common noise and pedestals were subtracted from the raw ADC values for each channel of a silicon layer. The residuals of each channel are scanned for signals larger than 5 times the rms of the channel pedestal. If this holds for a strip k, a charge cluster is defined to include all neighbors strips, provided their residual ADC content is larger than $2.5\,\sigma_{k\pm i}$. One more neighbor strip on each side is included if its residual ADC is larger than $1.5\,\sigma_{k\pm(i+1)}$. Only clusters with less than six strips went to the further analysis. A cluster is not formed if it would include a dead channel.

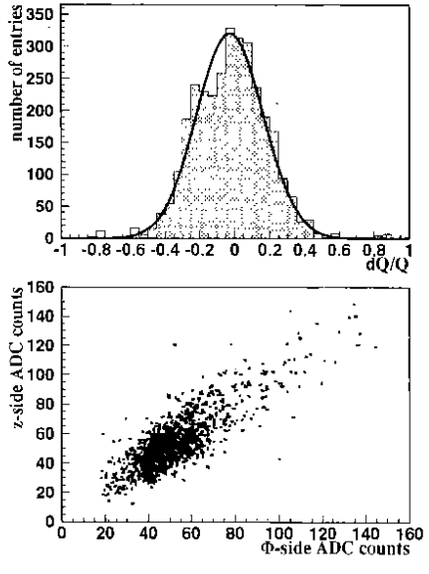

Figure 6: *Charge correlations between Φ and Z sides*

A qualitative justification of this algorithm is illustrated in Fig.6. The scatter plot of the measured cluster charges belonging to the same trigger Q_Φ and Q_Z from the Φ and Z layers, respectively, shows a linear correlation between the two charges ($\sigma_{cor} = 19\%$). This

is expected for double-sided sensors since a charged particle traversing the silicon sensor generates equal numbers of holes and electrons.

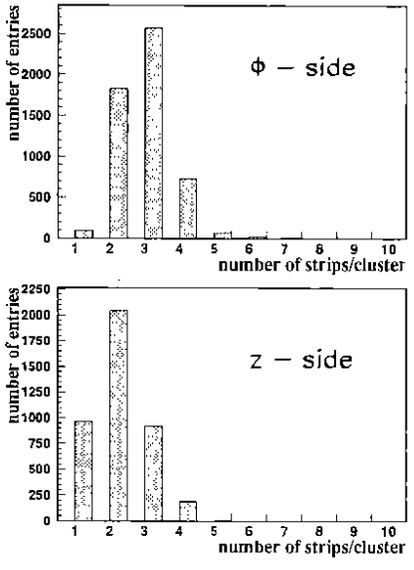

Figure 7: *Number of strips per cluster*

The distribution of the number of strips belonging to a cluster is shown in Fig. 7 for the Φ and Z layers for tracks which cross the modules at normal incidence. With the cluster definition as described above the average values for the cluster sizes are 3.1 and 2.3, respectively.

The dependence of the cluster size on the polar angle of the crossing track is shown in Fig. 8 for the Z layer. The observed increase with polar angle is expected since the projection of an incident particle's track onto the Z-side strips increases with increasing polar angle Θ. As expected no increase in the cluster size on the Φ side was found. The errors are statistical ones.

The signal to noise ratio S/N is an important quality measure of a module. We define it as $S/N = Q_{mp}/\sigma_{mean}$, where Q_{mp} is the most probable value of the cluster charge and σ_{mean} is

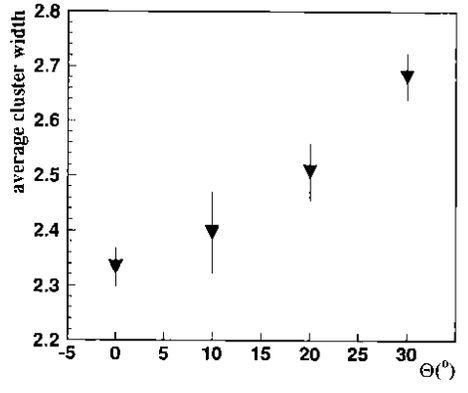

Figure 8: *The average Z side cluster size as a function of the polar angle Θ*

the mean value of the pedestal rms for the strips comprising the cluster.

The distributions of the total cluster charge for the Φ and Z layers are shown in Fig. 9. They qualitatively display a Landau shape. To determine Q_{mp}, fits to a convolution of a Landau distribution with a Gaussian distribution are performed. The resulting values for Q_{mp} are 43.8 and 43.2 ADC counts. With σ_{mean} values of 2.5 and 2.8, the S/N is 17.5 and 15.5 for the Φ and Z layers, respectively.

6.2 Spatial Resolution

The impact point of a beam particle is defined by the cluster position, a rough estimate of which is simply the cluster center of gravity. However, the charge deposited in the silicon is collected by the two nearest strips in a non-linear way depending on the relative position of the impact point [20]. We define the parameter $\eta = Q_l/(Q_l + Q_r)$, where Q_l and Q_r are, respectively, the charges collected on the left hand and right hand nearest strips.

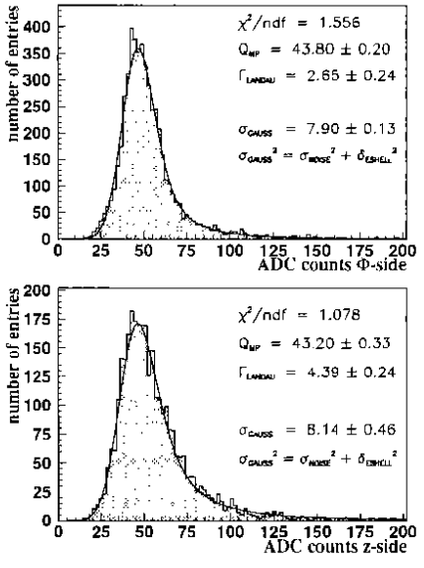

Figure 9. *Distribution of the total cluster charge for Φ and Z sides fitted by a convolution of a Landau and a Gauss function*

Since the beam spot size is much larger than the readout strip pitch, we assume a uniform irradiation of the strips and correct the hit position by constructing a rectifying function from the cumulative integral of $dN/d\eta$, where N is the number of counts whose charge is divided among the two strips.

A particle track is defined by the hits in the reference detectors upstream and downstream of the prototype detector. The spatial resolution of the prototype is determined by comparing the coordinates predicted by the reference detectors with those measured in the prototype detector. The distributions of the differences $\delta\Phi = \Phi_{ref} - \Phi_{meas}$ and $\delta Z = Z_{ref} - Z_{meas}$ are then fitted by a Gaussian distribution, as shown in fig. 10.

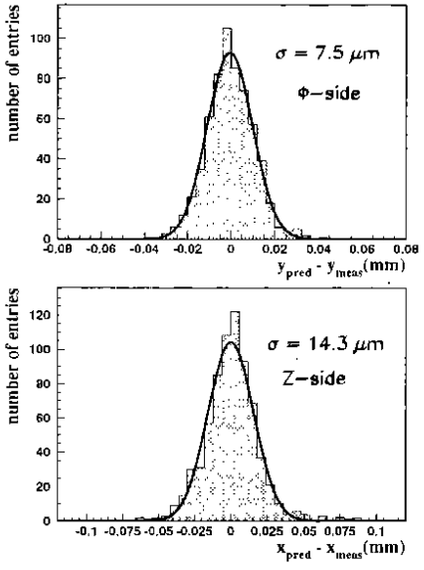

Figure 10: *Resolution of the prototype module for non-inclined tracks*

Subtracting in quadrature the estimated resolution of the reference detectors yields a spatial resolution for the prototype Φ and Z layers of $\sigma_\Phi = 7.5\,\mu$m and $\sigma_Z = 14.3\,\mu$m, respectively, for non-inclined tracks.

The dependence of σ_Z on the polar angle Θ is shown in Fig. 11. The resolution deteriorates for inclined tracks due to the increase in geometrical projection of the incident particle's track onto the Z side sensor plane. The resolution on the Φ side does not depend as expected from the polar angle of the track and is for all angles in the order of $8\,\mu$m.

6.3 Detection Efficiency

To calculate the detection efficiency ϵ, we consider a particle detected if in the corresponding detector layer a cluster is found at a position within $\pm 3\sigma_{\Phi,Z}$ of the predicted one. In this

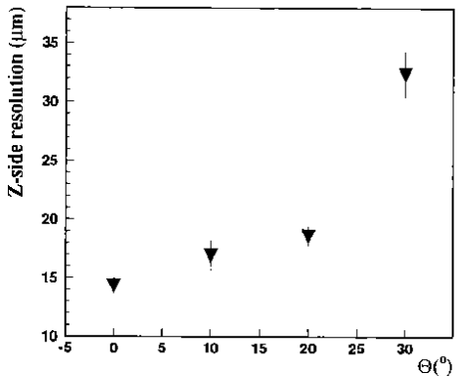

Figure 11: *The Z coordinate resolution as a function of the polar angle* Θ

case $\epsilon = 97\%$ for the Φ layer and $\epsilon = 96\%$ for the Z layer. If instead the cluster definition is changed to the requirement that a signal in some single channel be larger than 5 times the rms of the channel pedestal or two consecutive strips have a signal of more than 3 times the rms of their channel pedestal and that this signal be within four strips of the predicted impact point, the efficiency increases to $\epsilon = 99.9\%$ for the Φ layer and $\epsilon = 99.3\%$ for the Z layer.

6.4 Performance of the Displacement Monitoring Systems

The possible effect of the CDMS on SMD noise levels was measured by taking a sequence of SMD pedestal runs with the CDMS alternately switched on and off. The centroids and shapes of the pedestal distributions for the runs with the CDMS on were found to be practically identical to those observed for runs with the CDMS off. No noise induced in the SMD data by the CDMS was observed. The short-term behavior of the CDMS in the test beam environment is consistent which that observed in laboratory bench studies.

Laser light from the LDMS was successfully observed on the Φ-measuring strips. The centroid of the light spot was stable to $\sim 3\,\mu$m during the data taking period.

7 Acknowledgements

The project was supported in part by the German Bundesministerium für Forschung und Technologie, the Hungarian OTKA fund (contract No. 2970), the Italian Institute for Nuclear Physics, the Swiss National Science Foundation , the Taiwanese National Science Foundation and the United States Department of Energy (Grant No. DE-FG05-84ER40141, Task B). It is pleasure to thank L.Bosisio, C. Haber and P. Weilhammer for various discussions and suggestions during all phases of this work. We acknowledge the technical assistance of K.Ratz.

References

[1] H. Akbari et al., NIM A332 (1993) 33.

[2] K. Deiters et al., NIM A323 (1992) 162.

[3] L3 Collaboration, "Proposal for a Silicon Microvertex Detector for L3," CERN LEPC 91-5.
O. Adriani et al., Nucl. Phys. B (Proc. Suppl.) 32 (1993) 202.

[4] CSEM Recherche et Development, Neuchatel Switzerland.

[5] G.Bagliesi et al., INFN/PI AE 86/10.

[6] G.Ambrosi et al., Proc. of Experimental Apparatus for High Energy Physics and Astrophysics, San Miniato, Italy (1993) to be published in NIM.

[7] D.diBitonto et al., to be published in NIM A.

[8] S. Kleinfelder et al., IEEE Trans. NS-35 (1988) 171.

[9] United Technologies Microelectronics Center, Inc., Colorado.

[10] B.Bertucci et al., Proc. of Experimental Apparatus for High Energy Physics and Astrophysics, San Miniato, Italy (1993) to be published in NIM.

[11] O. Adriani et al., Nucl. Phys. B (Proc. Suppl.) 32 (1993) 480.

[12] V. Commichau, "User's Manual, Crate Master V02A," Second Edition, RWTH Aachen ,October 1987.

[13] V. Commichau, "User's Manual, DRP V05A," First Version, RWTH Aachen, March 1992.

[14] K. Hangarter, "Data Reduction Programs," Version 4N, RWTH Aachen, August 1993.

[15] F. Tonisch, "User's Manual, Sequencer," First Version, DESY-IfH Zeuthen, October 1993.

[16] Capacitec, Inc., Ayer, Massachusetts, USA.

[17] ADC (part no. E205), MUX (part no. E220), DSP Technology, Fremont, California, USA.

[18] R.Massetti, master theses University of Perugia, Italy (1993) and J.Wegmann, master theses University of Jena, FRG (1993)

[19] V. Chabaud et al., NIM A292 (1990) 75.

[20] E. Belau et al., NIM A214 (1983) 253.